Biochimica et Biophysica Acta, 1143 (1993) 223–234

BBABIO 43842

Stark effect (electroabsorption) spectroscopy of photosynthetic reaction centers at 1.5 K: evidence that the special pair has a large excited-state polarizability

Thomas R. Middendorf, Laura T. Mazzola, Kaiqin Lao, Martin A. Steffen and Steven G. Boxer

Department of Chemistry, Stanford University, Stanford, CA (USA)

(Received 1 October 1992)
(Revised manuscript received 19 January 1993)

Key words: Photosynthesis; Reaction center; Stark spectroscopy; Special pair

The Stark effect or electroabsorption spectrum of the Q_y transition of the special pair, P, of *Rb. sphaeroides* reaction centers has been measured at 1.5 K in frozen glycerol/buffer glasses. Under these conditions, inhomogeneous broadening of the absorption band is minimized, and some structure is resolved in the absorption and Stark effect spectra. As a result it is possible to greatly refine earlier analyses of Stark spectra which were obtained at higher temperatures in poly(vinyl alcohol) films. In addition to the substantial change in dipole moment which has been documented previously, the new data provide evidence for a substantial change in polarizability associated with the lowest electronic transition of P. It has generally been assumed that the dipolar character of *P results from mixing with charge-transfer states. It is shown that as a consequence of this same interaction, *P should be highly polarizable, consistent with the Stark data. This leads to the hypothesis that the observed substantial change in dipole moment is induced by the matrix electrostatic field in the vicinity of P. In this sense, the properties of *P are quite similar to those of carotenoid excited states in ordered protein matrices (Gottfried et al., Science (1991) 251, 662–665; Biochim. Biophys. Acta (1991) 1059, 76–90). The specific geometric arrangement of bacteriochlorophylls in the bacterial special pair results in a highly anisotropic excited-state polarizability which is very sensitive to environmental perturbation. The observed polarizability of *P can be used to estimate a likely lower limit for the matrix electrostatic field in the reaction center ($> 1.2 \cdot 10^6$ V/cm). It is expected that such a large electrostatic field plays an important role in determining the kinetics and thermodynamics of the initial electron transfer steps in photosynthesis.

Introduction

Electron transfer in photosynthetic reaction centers (RCs) is initiated by photoexcitation of a strongly interacting pair of bacteriochlorophyll (BChl) molecules referred to as the special pair or P. The mechanism of the initial light-driven charge separation step is still unresolved. One of the difficulties is that the initial state in this electron transfer reaction, the lowest singlet excited state of the special pair, ^{1}P, is still not well characterized. It is clear from electronic absorption, Stark [1–5], holeburning [6–15], and resonance Raman [16,17] spectroscopies that ^{1}P is very different from the excited singlet state of a monomeric BChl, whose properties are typical of most large aromatic chromophores. It is likely that these differences play a significant role in determining some of the unique features of the ultra-fast reaction dynamics in RCs.

Quantitative information on the electrostatic properties of excited electronic states can be obtained using the technique of Stark effect (electroabsorption) spectroscopy. The magnitude and line shape of the absorption change induced by an externally applied electric field can be related to fundamental molecular parameters such as the change in permanent dipole moment between the states connected by an optical transition. Thus, Stark spectroscopy is a particularly sensitive method for studying states with charge transfer (CT) character. The theory of electric field effects on molecular spectra has been developed in detail [18–21]. For an isotropic, immobilized sample the line shape of the field-induced change in absorbance can be described

Correspondence to: S.G. Boxer, Department of Chemistry, Stanford University, Stanford, CA 94305-5080, USA.

by a sum of the zeroth, first and second derivatives of the absorption spectrum:

$$\Delta A(\nu) = (f\mathbf{F}_{ext})^2\left\{A_\chi A(\nu) + \frac{B_\chi}{15hc}\frac{\nu\, d[A(\nu)/\nu]}{d\nu} + \frac{C_\chi}{30h^2c^2}\frac{\nu\, d^2[A(\nu)/\nu]}{d\nu^2}\right\} \quad (1)$$

where ν is energy in wavenumbers, h is Planck's constant, and c is the speed of light. The local field correction factor, f, relates the magnitude of the field present at the chromophore, $\mathbf{F}_{int}$, to that of the externally applied field: $\mathbf{F}_{int} = f \cdot \mathbf{F}_{ext}$. The coefficients A_χ, B_χ, and C_χ depend on molecular parameters such as the transition polarizability and hyperpolarizability *, the difference in polarizability $\Delta\boldsymbol{\alpha}$, and the change in permanent dipole moment $\Delta\boldsymbol{\mu}$, between the ground and excited electronic states connected by the optical transition that is being probed. In particular, the coefficient C_χ for the second derivative component is related to $\Delta\boldsymbol{\mu}$ as:

$$C_\chi = |\Delta\boldsymbol{\mu}|^2\{5 + (3\cos^2\chi - 1)(3\cos^2\zeta_A - 1)\} \quad (2)$$

where χ is the experimental angle between the electric vector of the linearly polarized probe light and the direction of the applied electric field, and χ_A is a molecular angle between $\Delta\boldsymbol{\mu}$ and the transition dipole moment, **p**.

Stark spectra of *Rb. sphaeroides* and *Rps. viridis* RCs in PVA films have been obtained at room temperature [1,2] and at 77 K [3–5]. The line shapes of the Stark spectra for the Q_y transitions of the special pair and the accessory bacteriochlorophyll and bacteriopheophytin chromophores are similar to the second derivatives of the corresponding absorption bands. Small deviations between the Stark line shape and the absorption second derivative for the P band were noted in these original reports, but were not considered in the data analysis. The large amplitude of the electric field effect for the P band indicates a large value of $|\Delta\boldsymbol{\mu}|$, estimated to be $\sim 7\ D/f$ (see below), for this transition. In addition, it was determined that the angle ζ_A is very different for P than for monomeric BChl in simple matrices. These results indicate that the electronic structure of the special pair is quite different from that of a monomeric BChl chromophore and that a substantial degree of charge separation has already occurred upon formation of ^{1}P. Furthermore, a large displacement of the vector $\Delta\boldsymbol{\mu}$ from the local C_2 axis of symmetry in the RC is observed, and this indicates that the electronic symmetry of ^{1}P is broken upon photoexcitation [22].

One of the difficulties of studying complex systems such as the RC is that the absorption bands, especially for P, are quite broad. Since the analysis of Stark data depends on comparisons with derivatives of the absorption spectrum, the inhomogeneous broadening can obscure important features. The resolution of the P band is significantly enhanced at 1.5 K because the band narrows and shifts to lower energy. In addition, the line width of this band at each temperature is significantly narrower in glycerol/buffer matrices than in PVA films [14], and there may be other consequences of using very dry PVA film samples [23]. Complications in the Stark spectrum due to overlap between neighboring transitions are therefore minimized by this choice of experimental conditions. The combination of the glassy matrix and extremely low temperature also has a pronounced effect on the line shape of the P absorption band. While nearly Gaussian at 77 K, the band is quite asymmetric at 1.5 K, revealing a shoulder on the low-energy side of the band. These features lead to a highly structured second derivative for the P Q_y absorption (vide infra). The strong temperature dependence of the absorption line shape provides a way to test the analysis of the earlier Stark measurements: if the Stark spectrum of the P band is dominated by the effect due to $\Delta\boldsymbol{\mu}$, then the line shape of this spectrum should change between 77 K and 1.5 K in a manner which is consistent with the changes in the second derivative of the absorption spectrum. This is found not to be the case (vide infra). A preliminary report of these results was presented elsewhere [24].

Materials and Methods

Wild type *Rb. sphaeroides* was grown semi-aerobically. RCs were obtained by standard methods [25], further purified by medium pressure liquid chromatography, and concentrated in Centricon-3 microconcentrators. RCs in 0.01% lauryldimethylamineoxide (LDAO) detergent, 10 mM Tris (pH 8), 20 mM NaCl were diluted with glycerol yielding a final solvent composition of 50% (v/v) glycerol/buffer. Final RC concentrations were typically $1 \cdot 10^{-4}$ M.

The RC samples were placed in glass sample cells with either semi-transparent Ni or indium tin oxide electrodes vacuum-deposited on the inner surfaces. Rapid immersion of the samples into a liquid He dewar containing a small amount of liquid N_2 produced glasses of good optical quality. After removal of the liquid N_2 by suction, the samples could be maintained at 77 K indefinitely by introducing He exchange gas into the area surrounding the sample to promote

* The electric field dependence of the transition moment **p** is characterized by the transition polarizability tensor **A** and the transition hyperpolarizability tensor **B** according to the relation: $\mathbf{p}(\mathbf{F}) = \mathbf{p}(\mathbf{F}=0) + \mathbf{A}\cdot\mathbf{F} + \mathbf{F}\cdot\mathbf{B}\cdot\mathbf{F}$.

thermal exchange with the outer liquid N_2 jacket of the dewar. By performing experiments at 77 K in this way, light scattering problems due to bubbling of liquid N_2 were avoided. The sample temperature was monitored continuously using a calibrated Si diode temperature sensor (DT471-DRC, Lake Shore Cryotronics) mounted in the sample holder. Experiments at 1.5 K were performed by introducing liquid He into the sample chamber followed by evaporative cooling of the He by mechanical pumping. The temperature was monitored by measuring the vapor pressure of the liquid He with a calibrated manometer (Validyne Engineering). Using this approach, we have obtained absorption and Stark spectra of frozen glass samples at 77 K and 1.5 K on the same sample under otherwise identical conditions.

Transmission spectra were obtained with light from a tungsten-halogen bulb passed through a 3/4 m double monochromator and detected with a Si avalanche photodiode (C30956E, RCA). Absorption spectra were obtained from transmission spectra of the samples and glycerol/buffer blanks which also contained Ni electrodes. The spectral resolution for the scans was typically 1.5 nm. Sinusoidal AC voltages were applied to the samples using a voltage amplifier of local design. The field-induced change in the sample transmission was detected at the second harmonic of the applied field frequency using locking detection. Electric fields on the order of 10^5 V/cm were routinely achieved in the stainless steel dewar. We are not aware that experiments of this type have previously been performed on frozen glasses at 1.5 K; however, this is the method of choice for a wide range of sample types.

One shortcoming of making measurements on frozen glasses is that it is much more difficult to obtain a precise estimate for the sample thickness compared to PVA film samples. In some cases, it is possible to observe interference fringes in thin samples, and this provides a very accurate measure of thickness in situ (Hug and Boxer, unpublished observations); however, in such cases it is nearly impossible to analyze the absorption spectrum and its derivatives because the fringes are comparable in magnitude to the absorption features. We have found that the difference between the thickness expected from the spacer and the actual thickness is often the result of differential pressure on the glass slides comprising the sample cell; this variation can be minimized. As a result of these difficulties, it is likely that the largest systematic error in these measurements comes from uncertainties in the thickness of the sample, and hence in the value for the applied electric field strength (the applied voltage is known with high accuracy). Examination of Eqn. 1 shows that this uncertainty will affect all contributions to the Stark effect in the same way. The central issue discussed in this paper is the relative contribution of the terms A_χ, B_χ and C_χ in Eqn. 1, and this is unaffected by systematic errors in the value of $\mathbf{F}_{ext}$, as well as the more fundamental uncertainty about the local field correction factor f.

For the angle measurements, it was necessary to use two polarizers to compensate for depolarization by the windows on the liquid He dewar at cryogenic temperatures. The probe light was initially polarized horizontally with a Glan-Thompson polarizer. A second polarizer (an IR film polarizer) was placed inside the sample compartment next to the glass slide before the sample cell. The probe light was polarized with a relative extinction of greater than 200:1 after it exited the liquid He dewar, as measured with a second Glan-Thompson polarizer. Identical results for the angle dependence of the electro-optic parameters at 77 K were obtained when the experiment was performed in a strain-free, quartz, optical liquid N_2 dewar, where the relative extinction of horizontal to vertically polarized light was $> 10^4$.

The experimental angle χ was determined by measuring the absorption spectrum at each angle. In order to change χ, the sample holder was rotated around a vertical axis, while the direction and polarization of the probe light were fixed. The ratio of absorption at each angle relative to that at $\chi = 90°$ was used to compute differences in path length, which in turn leads directly to the actual values of χ. This approach circumvents the need for specific knowledge of the refractive index of the glycerol/buffer solution as a function of temperature.

Results

Absorption, absorption second derivative, and Stark spectra of the Q_y region of wild type *Rb. sphaeroides* RCs in a 50% (v/v) glycerol/buffer glass at 77 K are shown in Fig. 1. The Stark spectrum has the approximate shape of the absorption second derivative for the P and accessory pigment bands. In comparison to the corresponding absorption second derivative, the amplitude of the features in the Stark spectrum of the P band are much larger than those for the accessory pigment Q_y transitions, suggesting that the value of $|\Delta\mu|$ must be considerably larger for the special pair. These observations are all in agreement with the previous Stark measurements on *Rb. sphaeroides* RCs in PVA films at 77 K [3–5].

Spectra for the identical sample at 1.5 K are shown in Fig. 2. The P, B, and H bands are narrower than at 77 K, as evidenced by the increase in the amplitude of the corresponding absorption second derivatives. The Stark spectra for the B and H monomer bands retain the approximate shape of the absorption second derivative at 1.5 K. In contrast, the Stark and second derivative line shapes for the special pair Q_y band are

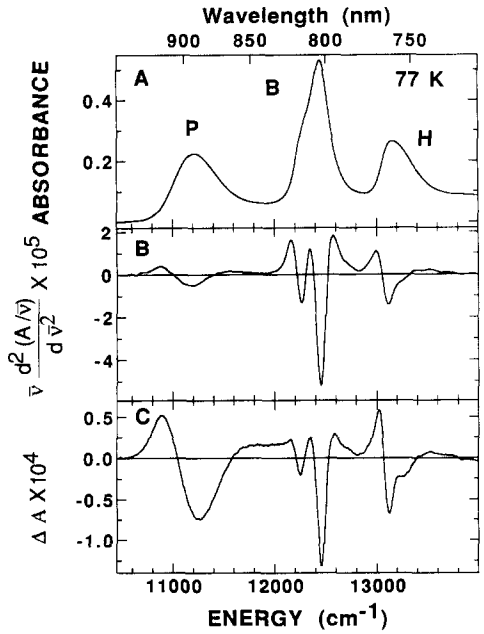

Fig. 1. Absorption (A), absorption second derivative (B), and Stark effect (C) spectra in the Q_y region of wild type *Rb. sphaeroides* RCs in a 50% (v/v) glycerol/buffer glass at 77 K. $F_{ext} = 9.90 \cdot 10^4$ V/cm, $\chi = 90°$.

very different at 1.5 K. In Fig. 3 the data for the P band are compared on an expanded wavenumber scale. The differences between the Stark spectrum and the second derivative are clearly seen. At both temperatures, the width between the zero-crossing points of the Stark spectrum is greater than that for the second

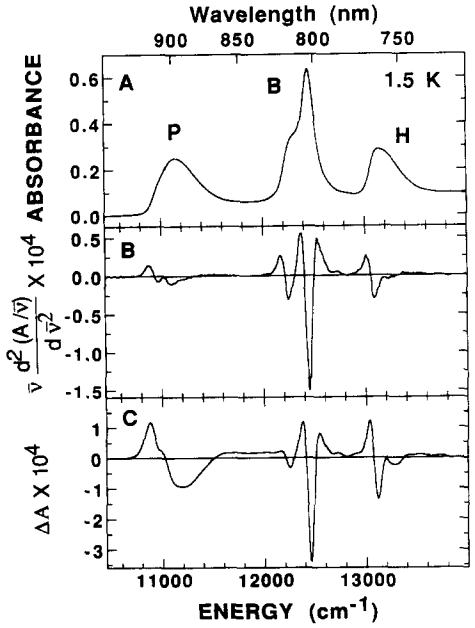

Fig. 2. Absorption (A), absorption second derivative (B), and Stark effect (C) spectra in the Q_y region of wild type *Rb. sphaeroides* RCs in a 50% (v/v) glycerol/buffer glass at 1.5 K. $F_{ext} = 9.90 \cdot 10^4$ V/cm, $\chi = 90°$. The spectra were taken on the identical sample as in Fig. 1.

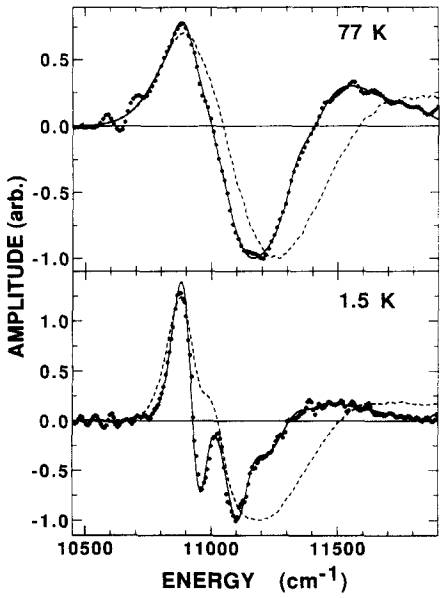

Fig. 3. Expanded view of the Stark spectrum (- - - - -) in the region of the Q_y absorption band of P in wild type *Rb. sphaeroides* RCs at 77 K and 1.5 K. Also shown is the second derivative of the absorption spectrum in this region (· · · · · ·), and the second derivative of a fit to the absorption spectrum at each temperature obtained using a sum of Gaussian functions which effectively smooths the absorption and leads to improved signal-to-noise in the derivatives (———). This latter approach can obscure features of high curvature; however, the comparison between the second derivative of the raw and smoothed absorption demonstrates that this smoothing is valid in this case. All spectra have been scaled to a magnitude of −1.0 at their respective minima to facilitate comparison.

derivative (536 vs. 409 cm^{-1} at 77 K; 484 vs. 382 cm^{-1} at 1.5 K). Additionally, the minima of the Stark spectra are blue-shifted relative to the minima of the second derivatives (85 cm^{-1} at 77 K; 120 cm^{-1} at 1.5 K). Similar but less-pronounced deviations had been noted for *Rb. sphaeroides* wild type and R-26 (carotenoidless) mutant RCs in PVA films at 77 K [3–5], but were partially obscured by the larger absorption line width in PVA. At 1.5 K, additional structure is present in the second derivative spectrum which is not seen in the Stark spectrum.

Stark spectra were also measured as a function of the angle χ, with χ varying from 90° to 55°. The analysis of these data depends on the model used to decompose the Stark effect line shape and is discussed in detail below. The field-dependence of the Stark spectrum of the P band was measured over a limited range. In contrast to PVA, frozen glass samples break down at rather low voltage; furthermore, we experienced difficulties due to arcing in our stainless steel liquid He dewar. The Stark effect line shape in glycerol/buffer at 1.5 K is independent of field strength, and the amplitude of the effect is quadratic with field strength to within 2% for applied fields ranging from $6.1 \cdot 10^4$ to $9.9 \cdot 10^4$ V/cm. Similar results were ob-

tained in measurements on RCs in PVA films at 77 K in fields as large as $2.5 \cdot 10^6$ V/cm (Lao, K. and Boxer, S.G., unpublished observations); however, because the line width in PVA is greater, it is a less sensitive probe.

Discussion

1. Stark line shape analysis

If the Stark effect on the Q_y absorption band of P is entirely due to the change in the permanent dipole moment between the ground state and ^{1}P, then Eqn. 1 predicts that the Stark spectrum should have the same line shape as the second derivative of the absorption spectrum at all temperatures. It is clear from the data in Fig. 3 that this is not the case for the P band. The simplest explanation for this finding is that effects due to the difference polarizability $\Delta\alpha$ and/or field-induced changes in the extinction coefficient contribute significantly to the Stark spectrum, adding components which have the line shape of the first and zeroth derivatives of the absorption spectrum, respectively. This possibility was investigated using two closely related methods of line shape analysis. For Method I, the absorption spectrum of the P band was fit over the range 11550–10450 cm^{-1} to a sum of Gaussian or higher-order Gaussian functions. The derivatives of the simulated spectrum were then computed and used to fit the Stark spectrum of the P band according to the equation:

$$\Delta A(\nu) = a_0 A(\nu) + a_1\left\{\frac{\nu\, d[A(\nu)/\nu]}{d\nu}\right\} + a_2\left\{\frac{\nu\, d^2[A(\nu)/\nu]}{d\nu^2}\right\} \quad (3)$$

using a least-squares algorithm. The fitting parameters are the weighting coefficients a_0, a_1 and a_2 for the derivative spectra. The derivative spectra obtained by this method were carefully checked against the derivatives of the experimental absorption spectra to ensure that they faithfully reproduced the true line shapes. The uniqueness of the fits to the Stark spectra was demonstrated by the fact that the coefficients obtained from the fitting procedure were unchanged for a wide range of initial values. Method II was similar to Method I, except that the absorption and Stark spectra were fit simultaneously, with the calculated deviation χ^2 for each spectrum weighted equally during minimization. The rationale behind Method II is that small errors in the measurement of the absorption spectrum will be amplified enormously in the derivative spectra, and thus small increases in χ^2 for the absorption fit may be offset by a better fit to the Stark spectra.

The results of the two line shape analysis methods are compared side-by-side in Figs. 4 (77 K data) and 5 (1.5 K data). The experimental and simulated absorption and Stark spectra are presented in the top two panels, respectively, and the contributions of the ze-

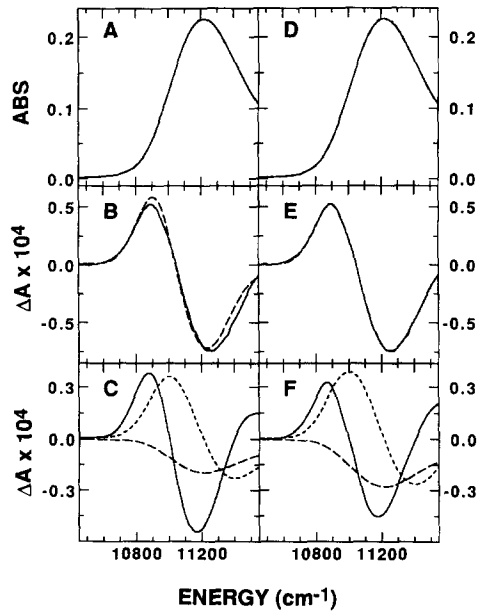

Fig. 4. Comparison of results of line shape analysis Method I (left panels A–C) and Method II (right panels D–F) applied to 77 K Stark effect data. Panels A and D, experimental (———) and simulated (— — —) absorption spectra; panels B and E, experimental (———) and simulated (— — —) Stark spectra; panels C and F, zeroth (— — —), first (- - - - -), and second (———) derivative contributions to Stark spectra.

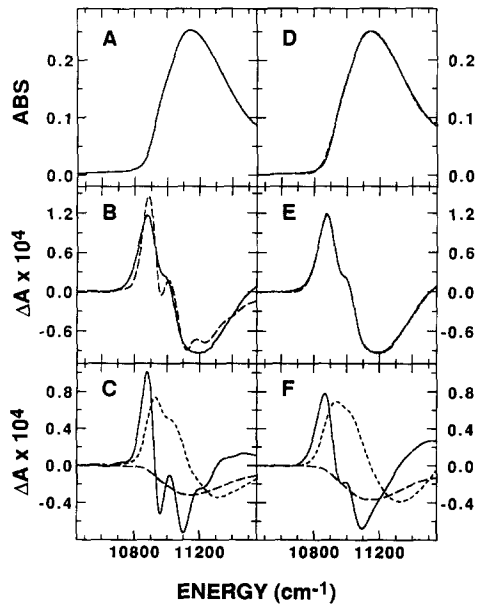

Fig. 5. Comparison of results of line shape analysis Method I (left panels A–C) and Method II (right panels D–F) applied to 1.5 K Stark effect data. Panels A and D, experimental (———) and simulated (— — —) absorption spectra; panels B and E, experimental (———) and simulated (— — —) Stark spectra; panels C and F, zeroth (— — —), first (- - - - -), and second (———) derivative contributions to Stark spectra.

roth, first and second derivatives of the absorption spectrum which best fit the Stark line shape are shown in the bottom panel. The fit to the absorption line shape using Method I is extremely good; however, significant deviations are observed between the experimental and simulated Stark line shape. It should be noted, however, that the latter fit is still superior to the second-derivative-only fit shown in Fig. 3. In contrast, the simultaneous fitting procedure (Method II) yields excellent fits to both the absorption and Stark spectra. Figs. 4 and 5 indicate that the Stark line shape can be modelled satisfactorily within the Liptay formalism; however, the fit requires significant contributions from all three absorption derivatives. One limitation of Method II is that the second derivative of the fit to the absorption spectrum differs significantly from the experimental second derivative. The latter agrees well with previously published spectra [26], indicating that the features in our experimental second derivative are real and reproducible. Thus it is possible that the better fit of the Stark spectrum using Method II is not significant. It should be noted, however, that despite the much better fit to the Stark spectrum with Method II, the relative contributions of the derivative spectra and the deduced values for the electro-optic parameters (see below) are quite similar for Methods I and II.

The values of the coefficient a_2 at different angles of χ for the second derivative contribution to the Stark line shape can be used to refine the previous estimates for the magnitude of $\Delta\mu$ and ζ_A (see Eqns. 1 and 2). At 77 K, analyses by Methods I and II yield values of $|\Delta\mu| = 5.3$ and 5.2 D/f, respectively. At 1.5 K, Methods I and II produce values of $|\Delta\mu| = 4.2$ and 4.7 D/f. It is likely that the lower estimate obtained by Method I is due to the increased sharpness of features in the second derivative, specifically the positive feature at $\sim 10\,880$ cm^{-1} and the negative feature at $\sim 11\,100$ cm^{-1}. These values can be compared to values for $|\Delta\mu|$ of 6.2 D/f at 77 K and 5.2 D/f at 1.5 K which are obtained if $|\Delta\mu|$ is estimated from the magnitude of the absorption second derivative only (i.e., a_0 and a_1 assumed equal to zero). Thus, the magnitude of $|\Delta\mu|$ is overestimated by about 15% if the zeroth and first derivative contributions to the Stark line shape are neglected in the analysis. As discussed in the Methods section, we note that there may be a systematic error in the absolute magnitude of the electro-optic parameters due to uncertainty in the sample thickness; however, this will not affect the relative contributions of the derivatives and derived electro-optic parameters.

It was reported earlier that ζ_A, the angle between the transition moment and $\Delta\mu$ for the P band of *Rb. sphaeroides* in PVA at 77 K is $38 \pm 2°$ [2–5]. This is the value for ζ_A which is obtained when the entire Stark line shape is considered to be due to a second-derivative contribution. When the same approximation is made, the value of ζ_A is found to be 37° for RCs in a glycerol/buffer glass as shown in Fig. 6A (open circles = 77 K, filled circles = 1.5 K). Because we can now see that there are substantial zeroth and first derivative contributions to the Stark line shape, it is possible to refine this treatment by analyzing the second-derivative components at different experimental angles χ. Stark spectra at each angle χ were decomposed into zeroth, first and second derivatives utilizing Method II. The ratios of the second-derivative components relative to that found at $\chi = 90°$, $\Delta A''(\chi)/\Delta A''(\chi = 90°)$, are plotted in Fig. 6A, along with Eqn. 2 evaluated for various values of ζ_A. A least-squares fit yields $\zeta_A = 43°$ at 77 K, and $\zeta_A = 47°$ at 1.5 K. Analysis of the 77 K data by Method I yielded the same value of ζ_A within experimental error; however, for the data at 1.5 K, analysis by Method I did not show good agreement with Eqn. 2.

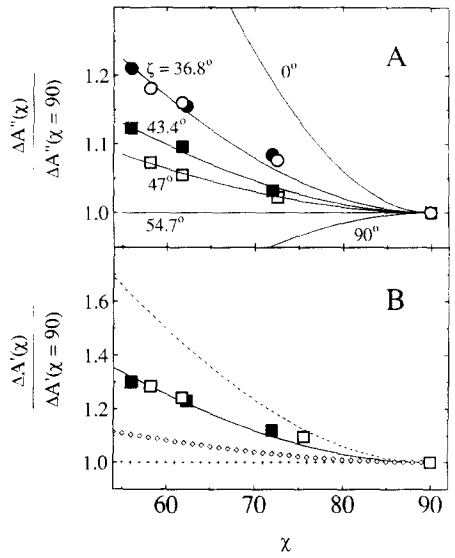

Fig. 6. (A) The χ dependence of the second derivative component of the Stark spectrum, plotted as the ratio of the second derivative contribution at a given value of χ relative to that at $\chi = 90°$, $\Delta A''(\chi)/\Delta A''(\chi = 90)$. Filled square symbols are for the second derivative contributions obtained from fits to the Stark spectrum using Method II at 77 K. Open square symbols are for the second derivative contributions at 1.5 K. Circle symbols are used for the ratios calculated with the assumption that ΔA is entirely due to second derivative effects (Filled circle, 77 K; open circle, 1.5 K). The solid lines are calculated according to Eqn. 2, evaluated for several values of ζ_A. (B) The χ dependence of the first derivative component of the Stark spectrum, plotted as the ratio of the first derivative contribution at a given value of χ relative to that at $\chi = 90°$, $\Delta A'(\chi)/\Delta A'(\chi = 90)$. Filled squares, 77 K; Open squares, 1.5 K. Calculated curves from Eqn. 4 are plotted for several values of the ratio $\Delta\alpha_p / Tr(\Delta\alpha)$. For a spherically symmetric polarizability tensor, this ratio is 0.33 (crosses); for $\Delta\alpha_{xx} = \Delta\alpha_{yy}$ and $\Delta\alpha_{zz} = 0$, this ratio has a maximum value of 0.5 (diamonds); for $\Delta\alpha_{xx} > 0$ and $\Delta\alpha_{yy} = \Delta\alpha_{zz} = 0$, this ratio has a maximum value of 1.0 (- - - - -). The solid line (———) is for the ratio 0.74.

A significant new result due to the improved resolution in glasses at low temperature and to the detailed line-shape analysis is the discovery of a large first-derivative component in the Stark spectrum of the Q_y band of P. Unlike the second-derivative term (Eqn. 2), which depends only on $|\Delta\boldsymbol{\mu}|$, the first-derivative or B_χ term in Eqn. 1 depends on several factors and is much more difficult to analyze with the information currently in hand [20,27]:

$$B_\chi = \tfrac{1}{2}[5\,Tr(\Delta\boldsymbol{\alpha}) + (3\cos^2\chi - 1)(3(\mathbf{p}\cdot\Delta\boldsymbol{\alpha}\cdot\mathbf{p}) - Tr(\Delta\boldsymbol{\alpha}))]$$
$$+ 10/p^2 \sum_{ij}[p_i A_{ij} \Delta\mu_j]$$
$$+ 3/p^2 \Big[(3\cos^2\chi - 1)\sum_{ij}(p_i A_{ji}\Delta\mu_j + p_i A_{jj}\Delta\mu_i$$
$$- \tfrac{2}{3}(p_i A_{ij}\Delta\mu_j)\Big] \qquad (4)$$

where $\mathbf{p}$ is a unit vector in the direction of the transition dipole moment and i, $j = x$, y, or z. We begin by ignoring contributions from the components of the transition moment polarizability A because we have no information on these contributions (they are likely to be small), and focus on obtaining an estimate for $Tr(\Delta\boldsymbol{\alpha})$ from the magnitude of the first derivative component. By measuring the relative contribution of the first derivative component at various values of χ, one can obtain the projection of $Tr(\Delta\boldsymbol{\alpha})$ along the transition dipole moment, denoted $\Delta\boldsymbol{\alpha}_p$. The results of such an analysis are depicted in Fig. 6B. Using Method II, at 77 K one obtains $Tr(\Delta\boldsymbol{\alpha}) = 930$ Å$^3/f^2$, and $\Delta\boldsymbol{\alpha}_p = 680$ Å$^3/f^2$, and at 1.5 K one obtains $Tr(\Delta\boldsymbol{\alpha}) = 1110$ Å$^3/f^2$ and $\Delta\boldsymbol{\alpha}_p = 840$ Å$^3/f^2$. In both cases, the ratio of $\Delta\boldsymbol{\alpha}_p/Tr(\Delta\boldsymbol{\alpha})$ is approx. 0.74. The large value for this ratio indicates that the difference polarizability $\Delta\boldsymbol{\alpha}$ lies largely along one of its principal molecular axes, and that the angle between this axis and $\mathbf{p}$ is less than 30°. One can not specify this angle with greater accuracy without specific knowledge of the individual diagonal elements of the polarizability tensor. However, even this limited information excludes some possibilities. For example, this large ratio precludes the possibility that $\Delta\boldsymbol{\alpha}$ is spherically symmetric. In this case, the ratio would be 0.33, and the first derivative contribution to the Stark spectrum as a function of χ would be constant; this is illustrated with the curve highlighted with crosses in Fig. 6B. The ratio is also too large for the polarizability to be equally distributed along two of the principal molecular axes, with a zero component along the third axis. In this case, the maximum possible ratio would be 0.5, and the χ-dependence would follow the curve highlighted with diamonds in Fig. 6B. If $\Delta\boldsymbol{\alpha}$ were entirely along one of the principal axes, and this axis were parallel to $\mathbf{p}$, the ratio would be 1.0, and the χ-dependence would follow the dashed curve in Fig. 6B. A ratio of less than 0.74 is obtained even if $\Delta\boldsymbol{\alpha}$ is entirely along one axis, but the angle between this axis and $\mathbf{p}$ is greater than 30°. From these limiting cases, one can conclude that the $\Delta\boldsymbol{\alpha}$ tensor is highly anisotropic, and its principal axis has a large projection along the transition moment.

The finding of such a large difference between the polarizability of the ground and lowest excited singlet state of the special pair is perhaps even more striking than the large difference dipole moment for the special pair. The large value of $Tr(\Delta\boldsymbol{\alpha})$ for P is 1–2 *orders of magnitude* larger than for other cyclic polyenes such as monomeric porphyrins [28] and chlorophylls [29,30] in solution, while $|\Delta\boldsymbol{\mu}|$ is ~ 2–3-times larger for P than for monomeric bacteriochlorophyll [3]. A recent study of a dimeric chlorophyll aggregate [29] indicates a significantly larger polarizability (~ 100 Å^3) than for a monomeric chlorophyll, and large, structure-dependent variations in the Stark spectum have been observed for several covalently connected chlorophylls [31]. Very large difference polarizabilities (several hundred Å^3) are more typical for linear polyenes [32,33] and for carotenoids [34,35] in condensed media (see below).

2. Mixing with CT states as the origin of the large polarizability

The origin of the large $\Delta\boldsymbol{\mu}$ for the P → ^{1}P transition in RCs has generally been attributed to the mixing of charge-transfer states with the lowest pure exciton state of P, which we shall label $^1P_{exc}$ [22,36]. What has not been widely appreciated is that such an explanation for the *dipolar* character of ^{1}P implies that ^{1}P is also highly *polarizable* [22,36]. This latter point is easily demonstrated using a simple perturbation theory [37] argument. * In the presence of an electric field $\mathbf{F}$, the

* The observables $\Delta\boldsymbol{\mu}$ and $\Delta\boldsymbol{\alpha}$ are differences between the dipole moments and polarizabilities, respectively, of the excited and ground electronic states. We do not have direct information on the dipole moment of the ground state of P; however, the following evidence suggests that it is small. We have observed that $|\Delta\boldsymbol{\mu}|$ for both the Q_x and Soret bands associated with the special pair are small [3], in contrast to the Q_y band. If P has a substantial ground state dipole moment, then the dipole moments for both the Q_x and the Soret bands (which share the same ground state) must also be large and parallel to the ground state dipole moment in order for the observed difference dipole to be small. Such a coincidence seems unlikely, leading to the reasonable suggestion that the dipole moment of the ground state of P is small, and it is the lowest singlet excited state which is unusually dipolar. In the case of $\Delta\boldsymbol{\alpha}$, it is difficult to propose a physical mechanism giving a very large ground state polarizability for P; therefore, $|\Delta\boldsymbol{\alpha}|$ will generally be ascribed exclusively to *P. A notable exception is azulene [27].

state $|\psi_F\rangle$ derived from the unperturbed state $|^1P_{exc}\rangle$ is given by:

$$|\psi_F\rangle = |^1P_{exc}\rangle - \sum_n \frac{\langle\phi_n|q\mathbf{R}\cdot\mathbf{F}|^1P_{exc}\rangle}{E(^1P_{exc}) - E(\phi_n)}|\phi_n\rangle \quad (5)$$

where the sum is over all of the other zeroth-order energy eigenstates ϕ_n, $E(^1P_{exc})$ and $E(\phi_n)$ are the energies of the states $|^1P_{exc}\rangle$ and $|\phi_n\rangle$, respectively, $\mathbf{R}$ refers to a sum over the coordinates of all of the electrons in the molecule, and q is the magnitude of the electronic charge. Eqn. 5 indicates that the field mixes the states $|\phi_n\rangle$ with $|^1P_{exc}\rangle$. The permanent electric dipole moment of the state $|\psi_F\rangle$ is given by

$$\mu(\psi_F) = \langle\psi_F|q\mathbf{R}|\psi_F\rangle. \quad (6)$$

Combining Eqns. 5 and 6, $\mu(\psi_F)$ can be expressed as:

$$\mu(\psi_F) = \mu(^1P_{exc}) - 2\sum_n \frac{\langle^1P_{exc}|q\mathbf{R}|\phi_n\rangle\langle\phi_n|q\mathbf{R}\cdot\mathbf{F}|^1P_{exc}\rangle}{E(^1P_{exc}) - E(\phi_n)} \quad (7)$$

where terms of order F^2 and higher have been neglected. The first term on the right hand side of Eqn. 7 is the intrinsic dipole moment of the state $^1P_{exc}$, while the second term represents an induced dipole moment $\mu_{ind} = \alpha\cdot\mathbf{F}$, where the elements α_{ij} $(i,j = x, y, \text{or } z)$ of the polarizability tensor are given by:

$$\alpha_{ij} = -2\sum_n \frac{\langle^1P_{exc}|q\mathbf{R}_i|\phi_n\rangle\langle\phi_n|q\mathbf{R}_j|^1P_{exc}\rangle}{E(^1P_{exc}) - E(\phi_n)} \quad (8)$$

where $\mathbf{R}_i$ and $\mathbf{R}_j = \mathbf{X}$, $\mathbf{Y}$, or $\mathbf{Z}$. Clearly, the polarizability is large if there is a significant mixing of states into ^1P that are dipole coupled to $^1P_{exc}$ (these may or may not be charge transfer states; see below). If $\mathbf{F}$ is an externally applied electric field, $\mathbf{F}_{ext}$, the induced dipole moment is oriented with respect to $\mathbf{F}_{ext}$, and gives rise to a unidirectional shift of the transition energies, leading to a first derivative feature in the Stark spectrum. However, the total electric field at the chromophore must also contain contributions from a matrix electric field, $\mathbf{F}_{matrix}$, of the RC protein, in addition to $\mathbf{F}_{ext}$. The expression *matrix field* is used to denote electric fields due to the constellation of charged, dipolar and polarizable groups within the RC protein. It should not be confused with the reaction field set up in response to the applied field; the matrix field is present even in the absence of any externally applied field. With $\mathbf{F} = \mathbf{F}_{ext} + \mathbf{F}_{matrix}$, the state $|\psi_F\rangle$ is characterized by two induced dipole moments, one due to the applied field, $\mu_{ind,ext} = \alpha\cdot\mathbf{F}_{ext}$, and one due to the matrix field, $\mu_{ind,matrix} = \alpha\cdot\mathbf{F}_{matrix}$. For an isotropic sample, $\mu_{ind,matrix}$ is distributed isotropically with respect to $\mathbf{F}_{ext}$, and thus gives rise to a second derivative line shape in the Stark spectrum that is indistinguishable from the effect due to an intrinsic permanent dipole moment of the same magnitude.

Recently, this phenomenon has been documented for carotenoids in photosynthetic antenna proteins [34,35]: the large polarizability difference [$Tr(\Delta\alpha) > 500$ Å$^3/f^2$] of the carotenoid spheroidene gives rise to an induced dipole moment of ~ 15 D/f when the chromophore is bound specifically in the B800–850 antenna protein. In that case, in contrast to the special pair, it is possible to extract the chromophore from the protein and study its Stark spectrum in a simple, disordered organic glass. As expected, the Stark spectrum in the non-polar matrix is dominated by a first derivative contribution, and the intrinsic value of $Tr(\Delta\alpha)$ can be reliably obtained (it is typical of other linear polyenes [33]). Using this intrinsic value of $Tr(\Delta\alpha)$, the large observed value of $\Delta\mu_{ind,matrix}$ induced by the protein matrix, and manifested as a dominant second derivative line shape in the Stark spectrum of a randomly oriented sample, can be used to estimate the magnitude of the matrix field which is on the order of $5\cdot10^6$ V/cm in the vicinity of spheroidene in the B800–850 complex. This is larger than the highest external applied fields that have been achieved, and therefore the first derivative contribution to the Stark lineshape due to the applied field is difficult to observe in the carotenoid-protein complex.

The large value of $Tr(\Delta\alpha)$ reported here for the special pair suggests that the large magnitude of $|\Delta\mu|$ for the special pair may have a similar origin. For the case of P, the induced dipole moment ($|\Delta\mu| \sim 5$ D/f) is substantially smaller than for spheroidene in the B800–850 complex ($|\Delta\mu| \sim 15$ D/f), and therefore the first derivative contribution can be readily seen in the Stark spectrum. Unlike spheroidene, P can not be extracted and studied in the absence of the RC protein (well-defined synthetic dimers have been investigated [31] and will be reported elsewhere). Because $Tr(\Delta\alpha)$ appears to be comparable for P and for the carotenoids, the smaller induced dipole moment for P may reflect a smaller magnitude of the matrix field in the vicinity of P as compared with spheroidene in the B800–850 complex, or it may result from a less favorable projection of the matrix field into the polarizability tensor of ^1P. In principle, it should be possible to extend this analysis by studying uniaxially oriented samples, and this is in progress.

It may seem odd to compare the properties of the special pair with those of carotenoids. The polarizabilities of simple cyclic polyenes such as porphyrins and chlorophylls are quite small, in contrast to those of linear polyenes, like carotenoids. However, the special pair consists of a strongly interacting pair of cyclic polyenes, and the data presented here suggest that such a pair, with its specific geometry, can have a polarizability which is as large or larger than that for a

linear polyene. As noted above, the angle-dependent Stark data suggest that the polarizability of ^1P is very anisotropic. Since the angle between the principal axis of $\Delta\alpha$ and the transition moment is small, and the orientation of the latter is known, we can relate the axis along which the polarizability is large to the structure of the special pair. This axis is the long axis of the special pair, corresponding to the nearly parallel *y*-axes of the bacteriochlorophyll monomers which are displaced relative to each other away from a face-to-face conformation. Interestingly, this is also the direction in which the π-electron system of the dimer is most extended, and in this respect the special pair is more carotenoid-like than monomeric cyclic polyenes or face-to-face cyclic polyene dimers. This analysis suggests a direct connection between the molecular geometry of the special pair (or any molecular dimer or higher aggregate) and the excited state polarizability. This may explain why such wide variations are observed in the Stark spectra of different antenna complexes which involve multiple chromophores [38] and synthetic chlorophyll dimers [31].

For molecular dimers it is natural to focus attention on the admixture of low-lying CT states. This is because, in a simple one-electron model, CT states involving movement of one electron from the HOMO of one molecule to the LUMO of the other are expected to be near in energy to the lowest-lying $\pi\pi^*$ transitions [22]. Previously, $|\Delta\mu|$ and ζ_A for the special pair have been interpreted explicitly in terms of the energies and dipole moments of CT states which are mixed into ^1P [22,36]. The model for the polarizability described above provides a simple physical framework for describing how the RC protein and the CT states of the RC chromophores may influence the magnitude and direction of $\Delta\mu$ for the special pair. If the excited-state dipole moment of ^1P is an induced dipole moment due to a matrix field of the RC protein, then $\mu(^1P)$ is given by $\alpha(^1P)\cdot\mathbf{F}_{\mathbf{matrix}}$. First, we consider the role of CT states. For each CT state that is mixed into ^1P, there will be a contribution to the polarizability like that described in Eqn. 8. For any given CT state, the denominator in Eqn. 8 indicates that the energy of $|CT\rangle$ relative to $|^1P_{exc}\rangle$ affects all of the α_{ij} equally. This energy difference thus affects the magnitude, but not the direction of $\mu(^1P)$. Since the direction of the transition moment for CT transitions generally lies along the direction of the permanent dipole moment of the CT state, then the magnitudes of the *X*-, *Y*-, and *Z*-polarized transition moment matrix elements between $|^1P_{exc}\rangle$ and $|CT\rangle$, and therefore the *relative* magnitudes of the α_{ij}, are determined by the orientation of $\mu(CT)$ in the molecular axis system. Thus the identity of the CT state which mixes with $^1P_{exc}$ affects the direction of $\mu(^1P)$ by preferentially increasing the size of specific components of $\alpha(^1P)$. Similar arguments apply if the states which mix into ^1P are not CT states; as in the case of CT states it is the magnitude and direction of the transition moments, $\langle^1P_{exc}|q\mathbf{R}|\phi_n\rangle$, which determine the magnitudes of the components of the α_{ij}. The protein affects $\mu(^1P)$ via the orientation and magnitude of $\mathbf{F}_{\mathbf{matrix}}$, which depends on the distribution of charged residues and dipolar and polarizable groups in the RC protein (these may be amino acids of the RC or solvent molecules). The matrix field may also affect $\mu(^1P)$ by raising or lowering the energies of CT states of the Rc chromophores. From this discussion, it is evident that these experiments could be used to map out the electrostatic nature of the interior of the RC protein if the components of $\Delta\alpha$ can be determined.

An estimate for the matrix field at the special pair can be obtained from the expression $\Delta\mu = \Delta\alpha\cdot\mathbf{F}_{\mathbf{matrix}}$, and the values of $|\Delta\mu|$ and $\mathrm{Tr}(\Delta\alpha)$ deduced from the Stark spectrum of P, if one assumes the following: (1) that $\Delta\mu$ arises entirely from the interaction between $\Delta\alpha$ and $\mathbf{F}_{\mathbf{matrix}}$, and (2) that $\Delta\alpha$ lies entirely along one of its principal axes, and that this axis is parallel to $\mathbf{F}_{\mathbf{matrix}}$. With these assumptions, one obtains $(\mathbf{F}_{\mathbf{matrix}})\cdot(\cos\theta) \simeq 1.2\cdot10^6$ V/cm (θ is the angle between $\mathbf{F}_{\mathbf{matrix}}$ and the molecular axis with non-zero polarizability). This represents a lower limit for $\mathbf{F}_{\mathbf{matrix}}$ in the vicinity of P. The estimate for $|\mathbf{F}_{\mathbf{matrix}}|$ will be larger if it is not parallel to the principal axis of $\Delta\alpha$, but the value of $(\mathbf{F}_{\mathbf{matrix}})\cdot(\cos\theta)$ is unchanged. The value of $\mathbf{F}_{\mathbf{matrix}}$ has implications for the relative energies of the intradimer CT state $P_L^+P_M^-$, and the symmetry related intradimer CT state $P_L^-P_M^+$, to the extent that these are the CT states primarily responsible for $\Delta\mu$ and $\Delta\alpha$ of the Q_y transition. If one assigns a value of 35 D to these CT states (estimated from the Mg–Mg distance [39–42]), then one of these states will be lowered in energy ~ 750 cm^{-1}, while the energy of the other will be raised ~ 750 cm^{-1}, relative to their values in vacuo. Thus the energy difference between P^+P^- and P^-P^+ will be ~ 1500 cm^{-1} due to interaction with the matrix field (distortions of the two macrocycles may affect the energy of these two states differentially). If $\mathbf{F}_{\mathbf{matrix}}$ is not parallel to the principal axis, the estimate for $|\mathbf{F}_{\mathbf{matrix}}|$ will be larger, but the energy splitting between the two CT states will not increase because $(\mathbf{F}_{\mathbf{matrix}})\cdot(\cos\theta)$ stays constant.

The notion of solvent symmetry breaking and matrix-induced dipoles in polarizable chromophores is well-documented for simpler systems [43]. A recent example is particularly relevant. Wild and co-workers [44] examined the dipole moment induced in a centrosymmetric chromophore. Such a chromophore should have zero dipole moment; however, a substantial change in dipole moment was observed for the lowest electronic transition, and $|\Delta\mu|$ was correlated with the solvent dielectric constant. Because the intrin-

sic polarizability of the chromophore was known independently, it was possible to estimate the magnitude of the matrix field. For the most polar matrix, poly(methylmethacrylate), the matrix electric field was estimated to be $2\text{–}3 \cdot 10^6$ V/cm. The interior of the RC is likely to be at least as polar as this polymer, and our lower limit estimate for the matrix field is around this value. Although the impact of the matrix field is only being detected indirectly via its effect on spectroscopic observables, it is interesting to speculate that the matrix field in the RC may affect electron transfer processes, perhaps as one of the determinants of unidirectionality. We know from other measurements that the rates and quantum yields of the initial electron transfer steps are greatly affected in applied electric fields on the order of $1\text{–}3 \cdot 10^6$ V/cm [23].

An important experimental observation which must be reproduced by any model for the electrostatic properties of ^{1}P is the absence of an external field dependence to the Stark line shape of the P band. To a first approximation, the field dependence of $\boldsymbol{\alpha}(^1\mathrm{P})$ can be estimated by modifying the denominator in Eqn. 8 to include the change in energy of the states $|\,^1\mathrm{P}_{\mathrm{exc}}\rangle$ and $|\phi_n\rangle$ due to the applied field. If the dipole moment of $|\phi_n\rangle$ is much larger than that for $|\,^1\mathrm{P}_{\mathrm{exc}}\rangle$, (i.e. $|\phi_n\rangle$ is a CT state), then this correction amounts to replacing the energy denominator by the expression $E(^1\mathrm{P}_{\mathrm{exc}}) - E(\mathrm{CT}) + \boldsymbol{\mu}(\mathrm{CT}) \cdot \mathbf{F}_{\mathbf{ext}}$. Thus, the polarizability of ^{1}P is itself field dependent. The relative change in the polarizability depends on the value of $\boldsymbol{\mu}(\mathrm{CT}) \cdot \mathbf{F}_{\mathbf{ext}}$ compared to the zero-field energy difference $E(^1\mathrm{P}_{\mathrm{exc}}) - E(\mathrm{CT})$. If $\boldsymbol{\alpha}(^1\mathrm{P})$ is significantly different for two values of the external field, then the Stark line shape will be different in these two fields, and the amplitude of the spectrum will not scale quadratically with applied field. Simulations of the external field dependence of the Stark spectrum using this model for the polarizability are shown in Fig. 7 for an isotropic sample of molecules with $\mathrm{Tr}(\boldsymbol{\Delta\alpha})$ and $\boldsymbol{\Delta\mu}$ similar to the values in Table I. The permanent dipole moment is assumed to arise entirely from the interaction of a matrix electric field with the molecular polarizability. The polarizability of ^{1}P is ascribed to mixing with a single CT state with a 35 D permanent dipole moment (equivalent to a full charge separated between the geometric centers of the bacteriochlorophyll monomers comprising the special pair). These simulations indicate that the Stark spectrum scales quadratically with applied field, and the line shape is independent of the applied field strength up to $1 \cdot 10^6$ V/cm, as long as the energy of the CT state differs from that of $|\,^1\mathrm{P}_{\mathrm{exc}}\rangle$ by more than about 2000 cm^{-1}. It should be noted that if a large matrix field is indeed present in RCs, then the energy difference between $|\,^1\mathrm{P}_{\mathrm{exc}}\rangle$ and $|\mathrm{CT}\rangle$ may be very different in the RC and in vacuum due to the perturbation $\mathbf{F}_{\mathbf{matrix}} \cdot \boldsymbol{\mu}(\mathrm{CT})$. If the states ϕ_n in Eqn. 8 do not have large permanent dipole moments or polarizabilities, then their energies will be essentially unchanged by the applied field, and the field dependence of the line shape will be even less than for the simulations in Fig. 7.

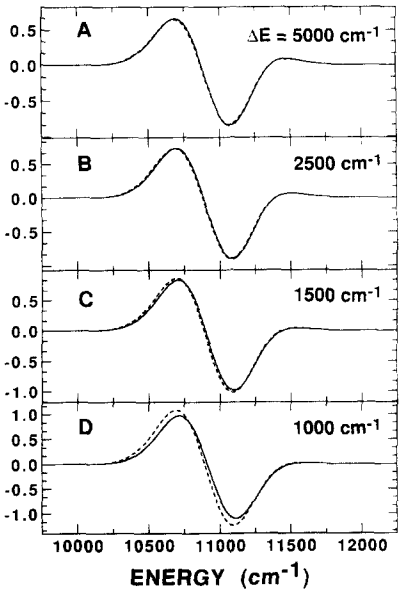

Fig. 7. Simulations of the external field dependence of the Stark line shape. The calculation is performed for an isotropic sample of molecules with a 500 cm^{-1} fwhm absorption spectrum which is entirely homogeneously broadened. The excited-state polarizability tensor is assumed isotropic with a trace of 500 Å^3 in the absence of an applied electric field, and the x, y, and z components of the matrix electric field are each set to $5 \cdot 10^6$ V/cm (this yields a matrix-field-induced dipole moment of 5 Debye). The external field dependence of the polarizability is calculated according to Eqn. 8 for energy gaps $E(^1\mathrm{P}_{\mathrm{exc}}) - E_{\mathrm{CT}}$ of (A) 5000 cm^{-1}, (B) 2500 cm^{-1}, (C) 1500 cm^{-1}, and (D) 1000 cm^{-1}. In each panel, the simulated spectrum is calculated for $F_{\mathrm{ext}} = 10^5$ V/cm (———) and 10^6 V/cm (- - - - - -). All spectra are divided by the square of the applied field strength to facilitate comparison of the line shapes.

TABLE I

Decomposition of Stark line shape of the special pair Q_y band in terms of absorption derivatives and derived electrooptic properties

Method	T (K)	$\lvert\boldsymbol{\Delta\mu}\rvert$ [a] (D/f)	$Tr(\boldsymbol{\Delta\alpha})$ [b] (Å^3/f^2)	ζ_A	$\boldsymbol{\Delta\alpha}_p$ (Å^3/f^2)
I	77	5.3±0.2	840± 90	45 ±20°	630± 70
II	77	5.2±0.15	930± 90	43.4± 1.5°	680± 70
I	1.5	4.2±0.3	700±200	– [c]	– [c]
II	1.5	4.7±0.15	1110±150	47.0± 1.5°	840±150

[a] 1 D = $3.34 \cdot 10^{-30}$ Cm.

[b] Contributions to the first derivative component of the Stark spectrum from effects involving the transition polarizability were ignored in the estimation of $Tr(\boldsymbol{\Delta\alpha})$ (see text). 1 Å^3 = $1.113 \cdot 10^{-40}$ Cm^2 V^{-1}.

[c] Not calculated (see text).

3. Possible shortcomings of conventional line shape analysis

We conclude by noting briefly a few potential complications in the analysis of the Stark spectrum of the special pair. The amplitude of the first derivative component of the Stark line shape contains contributions from cross-terms involving $\Delta\boldsymbol{\mu}$ and the components A_{ij} of the transition polarizability tensor **A** [27]. Without knowing the projections of $\Delta\boldsymbol{\mu}$ and **p** onto **A**, it is not possible to unambiguously determine these contributions. Some information on the magnitudes and relative signs of the A_{ij} can be obtained from the magnitude of the zeroth derivative component of the Stark spectrum; however, this component also contains contributions from the transition hyperpolarizability tensor. In the absence of specific information about these tensors, we simply note that under some conditions, the cross-terms involving $\Delta\boldsymbol{\mu}$ and **A** may make a significant positive contribution to the first derivative component of the Stark spectrum, which would have the effect of decreasing somewhat our estimate for the value of $Tr(\Delta\boldsymbol{\alpha})$. Experiments performed on uniaxially oriented RCs could potentially provide this information. In such an experiment one would detect the changes in ΔA at the fundamental frequency of the applied field. Contributions due to $\Delta\boldsymbol{\mu}$ would vary linearly with field and have a first derivative line shape, whereas contributions from **A** would be linear in field and give a zeroth derivative line shape.

Additional factors have been discussed in some detail in Ref. 35. They include the assumptions that $\Delta\boldsymbol{\mu}$, $\Delta\boldsymbol{\alpha}$, **A** and ζ_A for the transition are constant across the absorption band, and that there is only one electronic transition under the P band. The deviations between the simulated and experimental Stark spectra in Figs. 4 and 5 using Method I may be explained if either of these assumptions are not valid. The measurements of the χ-dependence of the Stark spectrum of RCs at 1.5 K provide no evidence for such an underlying structure. Finally, it is possible that some basic assumption underlying the derivation of Eqn. 1 is not valid. Recently, Reimers and Hush [45] have extended the original Liptay [19–21] treatment by explicitly including the effect of vibronic coupling. Under certain conditions, Stark line shapes are predicted which cannot be described by a simple sum of zeroth, first and second derivative contributions. Although we have no reason to challenge the classical model for electrochromic effects, speculation on the importance of vibronic coupling for the primary charge separation process has been presented by Won and Friesner [46]. Because low-lying CT states are an intrinsic property of dimers or higher aggregates of large aromatic molecules, and because these states are likely to mix significantly with locally excited or exciton states, we expect that the excited states of dimers should be much more polarizable than those of the constituent monomers. Therefore, the basic hypothesis that the matrix field induces a dipole moment in a polarizable chromophore, as demonstrated clearly for polyenes [34,35], is likely to be an important aspect of the properties of ^{1}P. With the exception of the prescient work of Scherer and Fischer [36], the polarizability has largely been ignored, but it may be a key to understanding the function of the special pair.

Acknowledgements

This work was supported in part by a grant from the NSF Biophysics Program. M.S. is the recipient of an MSTP Pre-doctoral Fellowship.

References

1 DeLeeuw, D., Malley, M., Butterman, G., Okamura, M.Y. and Feher, G. (1982) Biophys. Soc. Abstr. 37, 111a.
2 Lockhart, D.J. and Boxer, S.G. (1987) Biochemistry 26, 664–668; 2958.
3 Lockhart, D.J. and Boxer, S.G. (1988) Proc. Natl. Acad. Sci. USA 85, 107–111.
4 Lösche, M., Feher, G. and Okamura, M.Y. (1987) Proc. Natl. Acad. Sci. USA 84, 7537–7541.
5 Lösche, M., Feher, G. and Okamura, M.Y. (1988) in The Photosynthetic Bacterial Reacion Center—Structure and Dynamics (Breton, J. and Vermeglia, A., eds.), pp. 151–164, Plenum, New York.
6 Ganago, A.O., Melkozernov, A.N. and Shuvalov, V.A. (1986) Biophysics 31, 481–485.
7 Boxer, S.G., Lockhart, D.J. and Middendorf, T.R. (1986) Chem. Phys. Lett. 123, 476–482.
8 Boxer, S.G., Middendorf, T.R. and Lockhart, D.J. (1986) FEBS Lett. 200, 237–241.
9 Meech, S.R., Hoff, A.J. and Wiersma, D.A. (1985) Chem. Phys. Lett. 121, 287–292.
10 Meech, S.R., Hoff, A.J. and Wiersma, D.A. (1986) Proc. Natl. Acad. Sci. USA 83, 9464–9468.
11 Tang, D., Jankowiak, R., Gillie, J.K., Small, G.J. and Tiede, D.M. (1988) J. Phys. Chem. 92, 4012–4015.
12 Tang, D., Jankowiak, R. and Small, G.J. (1989) Chem. Phys. 131, 99.
13 Johnson, S.G., Tang, D., Jankowiak, R., Hayes, J.M., Small, G.J. and Tiede, D.M. (1989) J. Phys. Chem. 93, 5953–5957.
14 Johnson, S.G., Tang, D., Jankowiak, R., Hayes, J.M., Small, G.J. and Tiede, D.M. (1990) J. Phys. Chem. 94, 5849–5855.
15 Middendorf, T.R., Mazzola, L.T., Gaul, D., Schenck, C. and Boxer, S.G. (1991) J. Phys. Chem. 95, 10142–10151.
16 Shreve, A., Cherepy N., Franzen, S., Boxer, S.G. and Mathies, R. (1991) Proc. Natl. Acad. Sci. USA 88, 11207–11211.
17 Donohoe, R.J., Dyer, R.B., Swanson, B.I., Violette, C.A., Frank, H.A. and Bocian, D.F. (1990) J. Am. Chem. Soc. 112, 6716–6718.
18 Labhart, H. (1961) Chimia 15, 20–26.
19 Liptay, W. and Czekalla, J.Z. (1960) Z. Naturforsch. 15, 1072–1079.
20 Liptay, W. (1965) Z. Naturforsch. 20a, 272–289.
21 Liptay, W. (1974) in Excited States Vol. 1 (Lim, E.C., ed.), pp. 129–229, Academic Press, New York.
22 Boxer, S.G., Goldstein, R.A., Lockhart, D.J., Middendorf, T.R. and Takiff, L. (1989) J. Phys. Chem. 93, 8280–8294.
23 Boxer, S.G., Franzen, S., Lao, K., Stanley, R. and Stocker, J.S. (1992) in The Photosynthetic Bacterial Reaction Center II (Breton, J. and Vermeglio, A., eds.), pp. 271–282, Plenum, New York.

24 Mazzola, L.T., Middendorf, T.R., Boxer, S.G., Gaul, D. and Schenck, C.C. (1991) Biophys. J. 59, 139a (abstract).
25 Woodbury, N.W., Becker, M., Middendorf, D. and Parson, W.W. (1985) Biochemistry 24, 7516–7521.
26 Klevanik, A.V., Ganago, A.O., Shkuropatov, A.Ya. and Shuvalov, V.A. (1988) FEBS Lett. 237, 61–64.
27 Mathies, R.A. (1974) Ph.D. Thesis, Cornell University.
28 Davisson, A. (1980) Chem. Phys. 45, 409–414.
29 Krawczyk, S. (1991) Biochim. Biophys. Acta 1056, 64–70.
30 Gottfried, D.S. and Boxer, S.G. (1992) J. Luminesc. 51, 39–50.
31 Middendorf, T.R., (1991) Ph.D. Thesis, Stanford University.
32 Ponder, M. and Mathies, R. (1983) J. Phys. Chem. 87, 5090–5098.
33 Liptay, W., Wortmann, R., Bohm, R. and Detzer, N. (1988) Chem. Phys. 120, 439–448.
34 Gottfried, D.S., Steffen, M.A. and Boxer, S.G. (1991) Science 251, 662–665.
35 Gottfried, D.S., Steffen, M.A. and Boxer, S.G. (1991) Biochim. Biophys. Acta 1059, 76–90.
36 Scherer, P.O.J. and Fischer, S.F. (1986) Chem. Phys. Lett. 131, 153–159.
37 Cohen-Tannoudji, C., Diu, B. and Laloë, F. (1977) Quantum Mechanics, Vol. II, John Wiley & Sons, New York.
38 Gottfried, D.S., Stocker, J.S. and Boxer, S.G. (1991) Biochim. Biophys. Acta 1059, 63–75.
39 Deisenhofer, J., Epp., O., Miki, K., Huber, R. and Michel, H. (1984) J. Mol. Biol. 180, 385–398.
40 Deisenhofer, J., Epp., O., Miki, K., Huber, R. and Michel, H. (1985) Nature 318, 618–624.
41 Allen, J.P., Feher, G., Yeates, T.O., Komiya, H. and Rees, D.C. (1987) Proc. Natl. Acad. Sci. USA 84, 5730–5734.
42 Chang, C.H., El-Kabbani, O., Tiede, D., Norris, J.R. and Schiffer, M. (1991) Biochemistry 30, 5352–5360.
43 Rettig, W. (1986) Angew. Chem. Int. Ed. Engl. 25, 971–988.
44 Meixner, A.J., Renn, A. and Wild, U.P. (1992) Chem. Phys. Lett. 190, 75–82.
45 Reimers, J.R. and Hush, N.S. (1991) in Mixed-Valence Systems: Applications in Chemistry, Physics and Biology (Prassides, K., ed.), Kluwer Academic Publishers, Dordrecht, p. 29.
46 Won, Y. and Friesner, R.A. (1988) J. Phys. Chem. 92, 2214–2219.